J Biomol NMR (2015) 62:341–351
DOI 10.1007/s10858-015-9948-1

ARTICLE

Fractional enrichment of proteins using [2-^{13}C]-glycerol as the carbon source facilitates measurement of excited state ^{13}Cα chemical shifts with improved sensitivity

Alexandra Ahlner[1] · Cecilia Andresen[1] · Shahid N. Khan[1] · Lewis E. Kay[2,3] · Patrik Lundström[1]

Received: 9 April 2015 / Accepted: 13 May 2015 / Published online: 20 May 2015

Abstract A selective isotope labeling scheme based on the utilization of [2-^{13}C]-glycerol as the carbon source during protein overexpression has been evaluated for the measurement of excited state ^{13}Cα chemical shifts using Carr–Purcell–Meiboom–Gill (CPMG) relaxation dispersion (RD) experiments. As expected, the fractional incorporation of label at the Cα positions is increased two-fold relative to labeling schemes based on [2-^{13}C]-glucose, effectively doubling the sensitivity of NMR experiments. Applications to a binding reaction involving an SH3 domain from the protein Abp1p and a peptide from the protein Ark1p establish that accurate excited state ^{13}Cα chemical shifts can be obtained from RD experiments, with errors on the order of 0.06 ppm for exchange rates ranging from 100 to 1000 s^{-1}, despite the small fraction of ^{13}Cα–^{13}Cβ spin-pairs that are present for many residue types. The labeling approach described here should thus be attractive for studies of exchanging systems using ^{13}Cα spin probes.

Keywords CPMG · ^{13}Cα labeling · [2-^{13}C]-Glycerol · Excited states

Introduction

Recent developments in NMR methodology have facilitated structure calculations of small proteins using ^{13}Cα, ^{13}Cβ, ^{13}CO, ^{1}Hα, ^{1}HN and ^{15}N chemical shift restraints (Cavalli et al. 2007; Shen et al. 2008). This is an important advance since of all NMR parameters, chemical shifts are the most easily and accurately measured and they are available at an early stage in any analysis of NMR data. It was soon realized that this methodology could also be used to obtain structural models for 'invisible', transiently and sparsely populated protein states, once chemical shifts were available. New approaches have also been developed for measurement of such shifts (Hansen et al. 2008; Ishima et al. 2004; Ishima and Torchia 2003; Loria et al. 1999; Lundström et al. 2009a, b), focusing on CPMG RD experiments (Carr and Purcell 1954; Meiboom and Gill 1958). Analysis of CPMG RD profiles allows the determination of the magnitude of the difference in chemical shifts, $|\Delta\varpi|$, between NMR spins in exchanging ground ('visible') and excited ('invisible') states so long as the excited conformer is populated to at least 0.5 % with a millisecond lifetime (Palmer et al. 2001). Signs of $\Delta\varpi$ values can be determined by additional experiments (Auer et al. 2009; Skrynnikov et al. 2002), so that chemical shift assignments can be obtained for the excited state conformer. Atomic resolution structural models have now been reported for a number of such states (Bouvignies et al. 2011; Korzhnev et al. 2010; Neudecker et al. 2012;

Electronic supplementary material The online version of this article (doi:10.1007/s10858-015-9948-1) contains supplementary material, which is available to authorized users.

✉ Patrik Lundström
patlu@ifm.liu.se

[1] Division of Chemistry, Department of Physics, Chemistry and Biology, Linköping University, 58183 Linköping, Sweden

[2] Departments of Molecular Genetics, Biochemistry and Chemistry, One King's College Circle, The University of Toronto, Toronto, ON M5S 1A8, Canada

[3] Program in Molecular Structure and Function, Hospital for Sick Children, 555 University Avenue, Toronto, ON M5G 1X8, Canada

Vallurupalli et al. 2008) and the methodology has been extended further to include rare conformers of nucleic acids as well (Dethoff et al. 2012; Kimsey et al. 2015).

Key to the success of the CPMG-based structure approach has been the development of robust selective labeling schemes that significantly reduce problems associated with homonuclear scalar couplings (Lundström et al. 2009c). In this regard it has recently been shown that saturation transfer (CEST) methodology (Forsén and Hoffman 1963) is robust to such couplings (Bouvignies et al. 2014; Vallurupalli et al. 2013), however the exchange window for which CEST is of utility has a relatively low upper limit, typically ($k_{ex} \approx$ 20–500 s^{-1}), and CPMG RD remains the method of choice for studying conformational transitions that are faster (k_{ex} up to $\approx$2000 s^{-1}).

Most of the selective labeling strategies that have been employed in the production of protein samples for CPMG RD studies are based on the use of suitably labeled glucose as the sole carbon source (Lundström et al. 2009c). For example, it has been shown that the use of [2-^{13}C]-glucose during protein overexpression leads to ^{13}C enrichment levels at Cα positions of between 17 and 45 %, essentially without concomitant ^{13}C labeling of Cβ, for 17 residue types (Lundström et al. 2007). Accurate ^{13}Cα chemical shifts of sparsely populated protein conformations can be readily obtained using such labeled protein samples along with pulse schemes that have been designed with the labeling scheme in mind (Hansen et al. 2008). The principal weakness of this labeling method is that the theoretical maximum enrichment at Cα is only 50 %, reducing the sensitivity of the NMR experiments accordingly.

A carbon source that has already been used for other purposes in NMR protein applications (Castellani et al. 2002; LeMaster and Kushlan 1996) is [2-^{13}C]-glycerol and it is expected that this precursor would lead to a doubling of the fractional incorporation of ^{13}C label at Cα. Moreover, this sensitivity gain would not be incurred at extra cost since the prices of [2-^{13}C]-glycerol and [2-^{13}C]-glucose are similar. The purpose of the present study is to investigate the use of [2-^{13}C]-glycerol as the carbon source in protein overexpression to establish (i) whether ^{13}Cα incorporation levels are as expected, (ii) whether isolated ^{13}Cα positions can be obtained and (iii) whether accurate ^{13}Cα chemical shifts of protein excited states can be determined from CPMG RD experiments. As we show below, the incorporation level is indeed doubled compared to the use of [2-^{13}C]-glucose and the fraction of undesired ^{13}Cα-^{13}Cβ spin-pairs is sufficiently low so as not to interfere with accurate measurement of ^{13}Cα chemical shifts by CPMG RD.

Materials and methods

Protein samples

An SH3 domain from the yeast protein Abp1p (Drubin et al. 1990; Lila and Drubin 1997; Rath and Davidson 2000) was prepared by overexpression in BL21(DE3) cells. Freshly transformed colonies were transferred to 30 ml LB supplemented with 100 mg/l ampicillin and grown to $OD_{600} = 1.0$ at 37 °C in a shaking incubator. Cells were then pelleted and a fraction resuspended in 50 ml M9 medium supplemented with 0.5 g/l $^{15}NH_4Cl$, 3 g/l [2-^{13}C]-glycerol and 100 mg/l ampicillin to give a starting $OD_{600} = 0.15$. The cells were grown to $OD_{600} = 0.8$ (5 h) and this culture was subsequently poured into 450 ml of M9 medium of the identical composition and grown to $OD_{600} = 0.55$ (6 h). Overexpression was induced by addition of 1 mM isopropyl-β-D-1-thiogalactopyranoside (IPTG) and continued for 12 h at 16 °C. The cells were harvested by centrifugation and the protein was purified as described previously (Vallurupalli et al. 2007). The resulting NMR sample was 0.55 mM in protein, 50 mM NaP_i, pH 7.0, 100 mM NaCl, 1 mM EDTA and 200 μM NaN_3. The solvent was 90 % H_2O/10 % D_2O, 100 % D_2O for ^{15}N–^{1}H and ^{13}C–^{1}H correlation experiments, respectively.

NMR spectroscopy

NMR experiments were performed using Varian INOVA spectrometers operating at 14.1 T, 18.8 T and 21.2 T, equipped with cryogenically cooled (14.1 T) or room-temperature (18.8 T and 21.1 T) probe-heads. All measurements were performed at 25 °C. To determine the fractional ^{13}C incorporation at Cα positions, constant-time ^{13}C–^{1}H correlation spectra (Santoro and King 1992; Vuister and Bax 1992) were recorded for samples prepared with ^{15}N, [2-^{13}C]-glycerol (referred to as selectively labeled sample in what follows) and ^{15}N, U–^{13}C-glucose. The fraction of isolated ^{13}Cα nuclei for each amino acid was estimated by recording a non-constant-time ^{13}C–^{1}H HSQC with $t_{1,max} = 80$ ms for the selectively labeled sample.

A 17-residue fragment (KKTKPTPPPKPSHLKPK) from the protein Ark1p (Haynes et al. 2007), purchased from EZBiolab, was titrated into the selectively labeled Abp1p SH3 domain sample and the populations of free and bound states monitored by recording ^{15}N CPMG relaxation dispersion experiments at 14.1 T. The titration was stopped once a population of the bound state of approximately 8 % was reached. ^{13}Cα RD experiments were performed at 14.1 T and 18.8 T using a pulse

sequence described previously (Hansen et al. 2008). For the experiment at 14.1 T the constant-time CPMG relaxation delay was 16 ms and datasets with effective fields of 62.5, 125, 187.5, 250, 312.5, 375, 437.5, 500, 625, 750, 875, 1000 Hz were recorded while for the measurements at 18.8 T a relaxation delay of 20 ms and effective fields of 50, 100, 150, 200, 250, 300, 400, 500, 600, 700, 800, 1000 Hz were used. After initial ^{13}Cα RD experiments were completed, additional Ark1p peptide was titrated into the sample and the ^{13}Cα CPMG experiments were repeated (14.1 and 21.1 T) using a constant-time relaxation delay of 16 ms and effective fields as above. Uncertainties were estimated from duplicate data points (Korzhnev et al. 2004).

Data analysis

All data were processed with NMRpipe (Delaglio et al. 1995) and visualized with Sparky (T. D. Goddard and D. G. Kneller, SPARKY 3, University of California, San Francisco). Peak integration was performed using the software PINT (Ahlner et al. 2013). For every peak, the fractional incorporation of ^{13}C label at each Cα position, f, was calculated as $f = (I_S^C/I_U^C)/a, a = \left\langle \frac{I_S^N}{I_U^N} \right\rangle$, where I_S^C and I_U^C are the intensities of cross peaks in constant-time ^{13}C–^{1}H correlation spectra recorded on the selectively and uniformly labeled samples, respectively, and a was calculated by summing intensity ratios of corresponding peaks in both samples over all peaks in the spectra. The fraction of ^{13}Cα–^{13}Cβ spin-pairs at a given site was estimated by the ratio $I_d/(I_s + I_d)$, where I_s and I_d are the intensities of singlet and doublet components for a correlation in a non-constant-time ^{13}C–^{1}H correlation spectrum recorded on the selectively ^{13}C labeled sample.

Intensities in CPMG spectra were converted into effective transverse relaxation rates, as $R_{2,eff}(\nu_{CPMG}) = 1/T \ln(I_0/I(\nu_{CPMG}))$ where $I(\nu_{CPMG})$ is the intensity in spectra that include the constant-time delay of duration T, $\nu_{CPMG} = 1/(2 \cdot \tau_{cp})$, where τ_{cp} is the delay between successive refocusing pulses in the CPMG train, and I_0 is the intensity when the relaxation delay is omitted. Dispersions were fitted to a two-state exchange model using the software CATIA (http://pound.med.utoronto.ca/software.html). The data were initially fitted on a per-residue basis and t-tests (details are given in the Results and Discussion section) performed to establish the presence of chemical exchange. A value of $p < 0.01$ was considered significant. RD profiles for residues showing chemical exchange via the above criteria were fitted to a global two-state process to extract exchange parameters and values of $|\Delta\varpi|$.

Results and discussion

The fractional incorporation of ^{13}C at Cα is doubled compared with [2-^{13}C]-glucose

The biosynthesis of amino acids using [2-^{13}C]-glucose as the sole carbon source has been described before, in particular with respect to ^{13}C labeling at Cα positions in proteins (Lundström et al. 2007). The principal weakness of the [2-^{13}C]-glucose approach is that one of the two glyceraldehyde-3-phosphate molecules generated in glycolysis is unlabeled, thereby diluting the ^{13}C label that eventually ends up on Cα by a factor of two. By contrast, [2-^{13}C]-glycerol can be converted to glyceraldehyde-3-phosphate that is 100 % labeled at position 2. For residue types derived from glycolytic intermediates, the maximum incorporation at Cα positions is thus increased from 50 to 100 %. Similarly, oxaloacetate and acetyl-S-CoA that enter the TCA cycle are twice as enriched in ^{13}C (see Fig. 1 of Lundström et al. 2007). Thus, residues derived from the TCA cycle intermediates oxaloacetate and α-ketoglutarate (AKG) are expected to be twice as enriched with ^{13}C at Cα positions as well. The only amino acid for which the Cα position is not derived from glycolytic or TCA cycle intermediates is histidine. If [2-^{13}C]-glucose is used as the carbon source we have found that the fractional ^{13}C incorporation at Cα is 30 % (Lundström et al. 2007). In contrast, if [2-^{13}C]-glycerol is used, fusion of two such molecules leads to glucose that is labeled at position 5. Glucose labeled in this manner is converted to ribose-5-phosphate (R5P) via the pentose phosphate pathway, that is 100 % ^{13}C labeled at position 5. Since R5P is the precursor of the aliphatic backbone of histidine with C5 becoming Cα, histidine α-carbons are expected to be labeled close to 100 % if [2-^{13}C]-glycerol is used as the carbon source.

We have determined the fractional incorporation of ^{13}C at Cα positions by comparing peak intensities in ^{13}C–^{1}H correlation maps of selectively and uniformly ^{13}C enriched Abp1p SH3 domain samples (see "Materials and methods" section). The results are presented in Table 1 where the amino acids have been grouped based on the precursor(s) they are derived from. For comparison, the results obtained previously using [2-^{13}C]-glucose (Lundström et al. 2007) are also shown.

As expected, the fractional incorporation is almost exactly doubled for most residue types compared to the previous case where [2-^{13}C]-glucose was used. Since the expression levels are similar for both [2-^{13}C]-glucose and [2-^{13}C]-glycerol (Lundström et al. 2009c), the sensitivity in NMR experiments per unit weight carbon source is doubled if [2-^{13}C]-glycerol is chosen as the carbon source. In our analysis (Table 1) we obtained reliable results for 15 of the

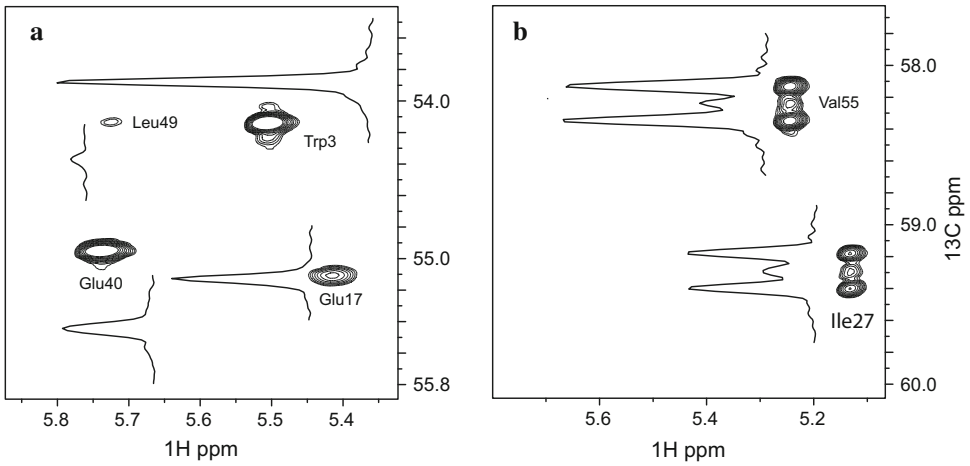

Fig. 1 Selected regions of non-constant-time ^{13}C-^{1}H HSQC spectra. Highlighted are a number of cross-peaks that show evidence of simultaneous ^{13}C labeling at Cα and Cβ positions, to an extent that varies with residue type. **a** Residue types for which ^{13}Cα–^{13}Cβ spin pairs are not predicted from the major biosynthetic pathways in isolation. **b** Residue types for which they can be predicted

Table 1 Fractional incorporation of ^{13}C label at protein Cα positions using [2-^{13}C]-glycerol and [2-^{13}C]-glucose

Precursor	Residue type(s)	Fractional incorporation [2-^{13}C]-glycerol[a]	Fractional incorporation [2-^{13}C]-glucose[b]
Pyruvate, phosphoenolpyruvate, 3-phosphoglycerate	Ala, Cys, Gly, Phe, Ser, Trp, Tyr, Val	0.94 ± 0.18 (9)	0.45 ± 0.04 (23)
Oxaloacetate	Asn, Asp, Ile, Met, Thr	0.66 ± 0.25 (5)	0.28 ± 0.02 (21)
α-Ketoglutarate	Arg, Gln, Glu, Pro	0.31 ± 0.08 (6)	0.17 ± 0.02 (17)
Oxaloacetate or pyruvate	Lys	0.77 ± n.a. (1)	0.38 ± 0.03 (11)
Ribose-5-phosphate	His	n.a.[c]	0.30 ± n.a. (1)
Acetyl-S-CoA	Leu	n.a.[d]	0.06 ± 0.01 (7)

[a] For an SH3 domain from yeast Abp1p (this work)

[b] For ubiquitin and an FF domain from human HYPA/FBP11 (Lundström et al. 2007)

[c] Not present in the SH3 domain from Abp1p

[d] Too low to be quantitated accurately

16 residue types present in the Abp1p SH3 domain, with the exception being Leu for which the fractional incorporation of ^{13}C was too low to quantitate accurately. For the residues not present in the domain (Arg, Cys, Gln and His), the incorporation level at Cα is expected to be very similar to that of other amino acids derived from AKG (Arg, Gln, ~30 %) or from pyruvate, phosphoenolpyruvate or 3-phosphoglycerate (Cys, ~90 %). As described above, the Cα position of His is expected to be labeled to almost 100 %.

It is also interesting to compare with previous results using similar labeling schemes. LeMaster and Kushlan used [2-^{13}C]-glycerol in combination with NaH^{13}CO$_3$ to express thioredoxin in cells with a disrupted TCA cycle (LeMaster and Kushlan 1996). The most striking difference is that Arg, Gln, Glu and Pro, are not labeled at all at Cα using their approach. This is entirely due to the lesion in the TCA cycle since only AKG produced in the second round of the cycle will produce residues labeled at Cα. A second difference is that Asn, Asp, Ile, Lys, Met and Thr are labeled >90 % at Cα compared to 66 % (77 % for Lys) here. Also in this case, the disrupted TCA cycle explains the differences as all oxaloacetate (OA) that is the precursor for these residue types must be derived from carboxylation of phosphoenolpyruvate and will be enriched for ^{13}C close to 100 % at the position corresponding to Cα if [2-^{13}C]-glycerol is used as the carbon source (Lundström et al. 2009b). Although cells with a disrupted TCA cycle increases the sensitivity slightly for six residue type this is offset by the loss of four potential probes for dynamics. In addition, cells with a disrupted TCA cycle are expected to grow slower and perhaps produce less protein. The use of NaH^{13}CO$_3$ by LeMaster and Kushlan is not expected to have any impact on labeling at Cα although it is beneficial for enrichment at other positions.

Key to the success of using [2-^{13}C]-glucose as the carbon source is the very low (in fact undetectable) fraction of ^{13}Cα–^{13}Cβ spin pairs for all residue types except isoleucine

and valine (Lundström et al. 2007). The reason for the need for isolated $^{13}C\alpha$ moieties is that the 35 Hz scalar coupling to Cβ during the constant time relaxation delay of a CPMG RD experiment will evolve differently depending on the repetition rate of the refocusing pulses. In the slow pulsing limit, the weak form of the scalar coupling applies and the scalar evolution of an operator I_Y^α is $I_Y^\alpha \rightarrow I_Y^\alpha \cdot \cos(\pi JT) - 2I_X^\alpha I_Z^\beta \sin(\pi JT)$ where I^β is the coupled spin, J is the coupling constant and T is the duration of the relaxation delay. In the fast pulsing limit, the evolution is instead $I_Y^\alpha \rightarrow I_Y^\alpha \cos^2(\pi JT) + I_Y^\beta \sin^2(\pi JT) + (I_Z^\alpha I_X^\beta - I_X^\alpha I_Z^\beta) \sin(2\pi JT)$. The evolution is thus modulated by the pulsing rate even in the absence of chemical exchange, leading to artifacts in RD profiles as has been reported before (Ishima and Torchia 2003).

Non constant-time ^{13}C–^{1}H HSQC spectra of the Abp1p SH3 domain generated using [2-^{13}C]-glycerol (Fig. 1) clearly show that there are additional residue types that are fractionally $^{13}C\alpha$–$^{13}C\beta$ labeled as can be seen from peaks that comprise a superposition of a singlet (corresponding to an isolated $^{13}C\alpha$ moiety) and a doublet (corresponding to a $^{13}C\alpha$–$^{13}C\beta$ spin pair). We quantified the percentage of $^{13}C\alpha$–$^{13}C\beta$ spin pairs (see "Materials and methods") and found that, as before, Cα and Cβ are simultaneously ^{13}C labeled in Ile and Val to approximately 85 %. For Ser and Trp (and we anticipate Cys) we quantify 9 % while for Ala, Glu and Asp, values of 8, 6 and 6 % are measured, respectively. Since the doublet components were often not well resolved from the center line the results must be interpreted as approximate. Moreover, only a subset of residues could be quantified, however, it is clear that a low, but measurable, level of spin pairs is produced.

A thorough analysis of the interplay between different metabolic pathways readily explains the results for many amino acids. If [2-^{13}C]-glycerol is used as the carbon source, two products of the pentose phosphate pathway are [1,5-$^{13}C_2$]-fructose-6-phosphate and [1,3,5-$^{13}C_3$]-fructose-6-phosphate, Fig. 2a. Subsequently, when these molecules enter glycolysis, Fig. 2b, the resulting three-carbon amino acids, such as serine, can be labeled at Cβ but not at Cα. The $^{13}C\beta$ of serine can then be transferred to tetrahydrofolate (THF) to yield N^5,N^{10}-methylene-THF and glycine, Fig. 2c. When the ^{13}C labeled methylene group of N^5,N^{10}-methylene-THF is transferred back to glycine, labeled with ^{13}C at the α-position, serine that is simultaneously labeled with ^{13}C at Cα and Cβ results. Since cysteine and tryptophan are derived from serine the same labeling pattern results for these amino acids. [1,5-$^{13}C_2$]-fructose-6-phosphate and [1,3,5-$^{13}C_3$]-fructose-6-phosphate are the source of [1-^{13}C]-acetyl-CoA (Fig. 2a) that can combine with [2-^{13}C]-oxaloacetate and enter the TCA cycle, Fig. 2d (Pass 1). The result is production of oxaloacetate (OA) ^{13}C labeled at C2 and C3 that in turn leads to $^{13}C\alpha$-$^{13}C\beta$ spin pairs for OA precursor amino acids Asn, Asp, Ile, Lys, Met and Thr. In a second round of the TCA cycle (Fig. 2d, Pass 2) OA labeled at C2 and C3 produces 2,3,4-^{13}C AKG that is the source of Arg, Gln, Glu and Pro, ^{13}C labeled at Cα and Cβ. Finally, the small amount of fractional $^{13}C\alpha$–$^{13}C\beta$ labeling for alanine can be understood from the fact that this residue can be formed as a degradation product of tryptophan (Voet and Voet 1995). Although similar possibilities for $^{13}C\alpha$–$^{13}C\beta$ labeling are expected when [2-^{13}C]-glucose is used as the carbon source during protein overexpression, it is clear that such effects are smaller and they were not detected in our previous analysis (Lundström et al. 2007).

In addition to scalar couplings to Cβ, also the effect of long range couplings must be considered. Although they are smaller they could still manifest as artifacts in RD experiments if the positions are sufficiently enriched for ^{13}C. We have not attempted to quantitate simultaneous labeling at Cα and other carbon positions with ^{13}C but Fig. 2d predicts simultaneous labeling at Cγ for residue types derived from OA and AKG. In addition, other positions, such as Cγ for aromatic residue types, are also predicted to be simultaneously labeled (Lundström et al. 2007). In many of these cases, the coupled nuclei resonate sufficiently far from $^{13}C\alpha$ so that couplings can be refocused by substituting band-selective pulses (Geen and Freeman 1991) for hard pulses in the CPMG pulse train. Couplings to aliphatic carbons of residues derived from AKG (Arg, Gln, Glu and Pro) are however hard to refocus this way and may still lead to artifacts.

Accurate protein excited state $^{13}C\alpha$ chemical shifts can be obtained

As described above, the principle advantage of using [2-^{13}C]-glycerol to produce proteins for $^{13}C\alpha$ CPMG RD studies is the two-fold increase in fractional incorporation of ^{13}C at Cα relative to what is obtained when [2-^{13}C]-glucose is used as the carbon source. This gain is offset to some extent by the increase in $^{13}C\alpha$–$^{13}C\beta$ spin pairs that, in turn, compromises the utility of RD profiles due to magnetization interchange between the coupled $^{13}C\alpha$, $^{13}C\beta$ spins during application of the CPMG pulse train (Ishima et al. 2004; Lundström et al. 2008, 2009a). We have therefore extensively evaluated the utility of the [2-^{13}C]-glycerol labeling scheme in $^{13}C\alpha$ RD studies. This was achieved by using an exchanging system described previously (Hansen et al. 2008; Vallurupalli et al. 2007) involving an SH3 domain from the yeast protein Abp1p (Drubin et al. 1990; Lila and Drubin 1997; Rath and Davidson 2000) and a peptide from the protein Ark1p (Haynes et al. 2007),

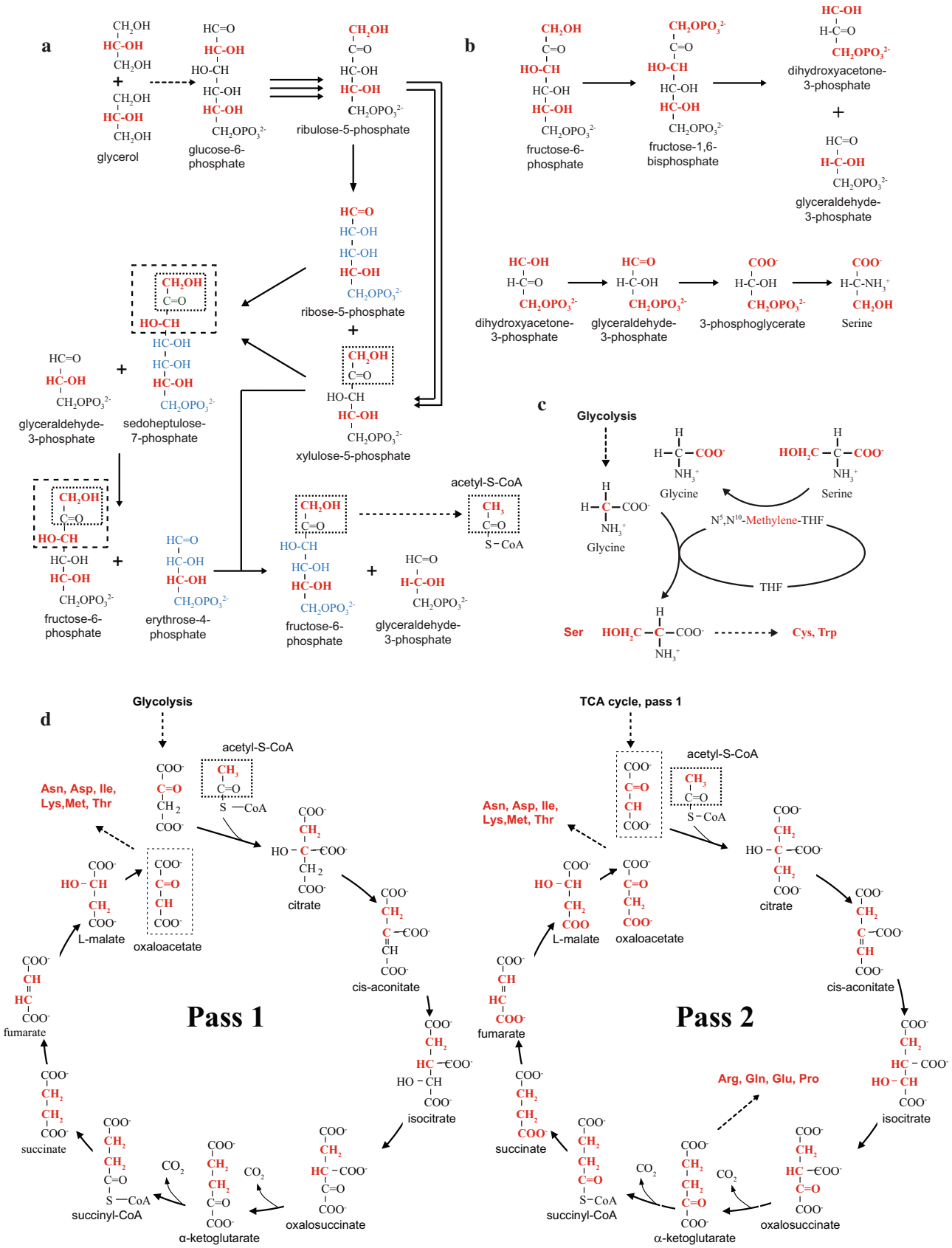
a
glycerol
glucose-6-phosphate
ribulose-5-phosphate
ribose-5-phosphate
xylulose-5-phosphate
glyceraldehyde-3-phosphate
sedoheptulose-7-phosphate
fructose-6-phosphate
erythrose-4-phosphate
fructose-6-phosphate
glyceraldehyde-3-phosphate
acetyl-S-CoA
b
fructose-6-phosphate
fructose-1,6-bisphosphate
dihydroxyacetone-3-phosphate
glyceraldehyde-3-phosphate
dihydroxyacetone-3-phosphate
glyceraldehyde-3-phosphate
3-phosphoglycerate
Serine
c
Glycolysis
Glycine
Serine
Glycine
N5,N10-Methylene-THF
THF
Ser
Cys, Trp
d
Glycolysis
acetyl-S-CoA
Asn, Asp, Ile, Lys,Met, Thr
citrate
L-malate
oxaloacetate
cis-aconitate
fumarate
isocitrate
succinate
succinyl-CoA
α-ketoglutarate
oxalosuccinate
CO2
Pass 1
TCA cycle, pass 1
acetyl-S-CoA
Asn, Asp, Ile, Lys,Met, Thr
citrate
L-malate
oxaloacetate
cis-aconitate
fumarate
isocitrate
succinate
succinyl-CoA
α-ketoglutarate
oxalosuccinate
Arg, Gln, Glu, Pro
CO2
Pass 2

◀**Fig. 2** Interplay of biosynthetic pathways leading to $^{13}C\alpha$–$^{13}C\beta$ spin pairs when [2-^{13}C]-glycerol is the carbon source during protein overexpression. ^{13}C labeled positions are highlighted in *red*. *Other colors* and *boxes* are used to track the fate of specific fragments. Amino acids that are simultaneously labeled at Cα and Cβ are shown in *red font*. *Dashed arrows* indicate reactions that proceed in several steps. *Multiple solid arrows* indicate that a number of product molecules are produced that are then used as reactants in different steps along the cycle. For example, three molecules of glucose-6-phosphate are converted into three molecules of ribulose-5-phosphate (hence three *solid arrows*), one of which is then converted into ribose-5-phosphate and two into xylulose-5-phosphate. **a** The pentose phosphate pathway starting from [2-^{13}C]-glycerol leads to the synthesis of [1,5-$^{13}C_2$]- and [1,3,5-$^{13}C_3$]-fructose-6-phosphate. **b** Fructose-6-phosphate from the pentose phosphate pathway enters glycolysis, producing Ser that is ^{13}C labeled at the CO and Cβ positions, but not at Cα. **c** Synthesis of $^{13}C\alpha$–$^{13}C\beta$ labeled serine, cysteine and tryptophan from fructose-6-phosphate derived from the pentose phosphate pathway and glycine derived from glycolysis. **d** Two passes of the TCA cycle, in which oxaloacetate at the start of the first pass is derived from glycolysis and acetyl-S-CoA is derived from fructose-6-phosphate synthesized in the pentose phosphate pathway. The first pass (Pass 1) leads to $^{13}C\alpha$–$^{13}C\beta$ spin pairs in residues derived from oxaloacetate, while a similar scenario occurs for amino acids from α-ketoglutarate in the second pass (Pass 2)

SH3 + Ark1p peptide $\rightleftarrows$ *SH3*-peptide

The dissociation constant for the complex is 0.55 μM, 25 °C (Vallurupalli et al. 2007) and the exchange kinetics are such that the pseudo first-order rate constant, $k_{ex} = k_{on}[L] + k_{off}$ where $[L]$ is the concentration of free Ark1p peptide, can be varied over the range of 'CPMG sensitive exchange rates' (approximately 100–2000 s^{-1}) simply through the addition of different amounts of Ark1p peptide. Further, when only a small amount of peptide is added, the major conformation in solution is the unbound SH3 domain ('ground state'), while the minor conformer ('excited state') is the bound domain. The situation is reversed through the addition of close to stoichiometric amounts of peptide. Because it is possible to prepare samples of free and fully bound SH3 domain, the chemical shifts of both states can be determined using conventional NMR methods to high accuracy, providing a benchmark for the corresponding values obtained by CPMG RD methods.

Initially, Ark1p peptide was titrated into a solution of free SH3 domain to yield a population of bound SH3 domain, p_B, of 8.3 ± 0.3 % and $k_{ex} = 138 \pm 9$ s^{-1}, as established from ^{15}N CPMG experiments recorded at 14.1 T. Subsequently, $^{13}C\alpha$ CPMG dispersion profiles were recorded at 14.1 and 18.8 T, so that absolute values of shift differences obtained either via CPMG ($|\Delta\varpi_{CPMG}|$) or directly from spectra of bound and free SH3 domain ($|\Delta\varpi_{Direct}|$) could be compared. Since many alpha protons resonate close to water the sample was lyophilized and dissolved in 99 % D_2O prior to recording $^{13}C\alpha$ RD experiments.

Accurate values of $|\Delta\varpi_{CPMG}|$ can be obtained from fits of RD profiles only if p_B, k_{ex} can be quantified properly. This is most easily accomplished by initially including only residues in fits (i) for which RD profiles show significant chemical exchange and (ii) where systematic errors are minimal. Thus, we have excluded Ile and Val residues from analysis because of the high fraction of $^{13}C\alpha$–$^{13}C\beta$ spin pairs for these amino acids, as well as Leu because of the low fractional incorporation of ^{13}C label at the Cα position (Fig. 1a). RD profiles from Gly have also been excluded because the methylene spin system at Cα requires a different pulse scheme than the one used here for the methine Cα positions (Lundström et al. 2009b; Mulder et al. 2001). There are a number of approaches for identifying candidate RD profiles for analysis. The most straightforward method is to use a minimum cutoff for the size of the profiles, as described previously (Choy et al. 2005). Another method is to fit the data on a residue-by-residue basis to models that either include or exclude chemical exchange and then use an F-test statistical analysis to select the appropriate model. Here we have used a simple, alternative method. For chemical exchange on all time-scales the effective transverse relaxation rate, $R_{2,eff}$, in single quantum CPMG RD profiles is higher in the free precession limit ($\nu_{CPMG} \rightarrow 0$) than for fast-pulsing ($\nu_{CPMG} \rightarrow \infty$). $R_{ex}(\nu_{CPMG}) = R_{2,eff}(\nu_{CPMG}) - R_{2,eff}(\nu_{CPMG} \rightarrow \infty)$ is thus a decaying function and under conditions of intermediate to fast exchange it decays monotonically and can be approximated by a decaying exponential for which the logarithm is linear in ν_{CPMG}. Thus, the presence of exchange can be established by fitting $\log[R_{ex}(\nu_{CPMG})]$ values to a linear function and testing the resulting slopes to see if they are different from zero. The protocol we have used is thus: (i) fit RD curves on a residue-by-residue basis, (ii) subtract the exchange-free contribution and calculate the logarithm, (iii) fit to a linear function and (iv) perform a t-test to determine whether the slope is different from zero. Using this protocol and considering a significance level of $p < 0.01$ we identified chemical exchange at $^{13}C\alpha$ positions for 17 residues. These included all amino acids for which $|\Delta\varpi_{Direct}| > 0.2$ ppm but not three of the residues with 0.1 ppm $< |\Delta\varpi_{Direct}| < 0.2$ ppm. In addition, $^{13}C\alpha$ nuclei for two residues for which $|\Delta\varpi_{Direct}| < 0.05$ ppm were likely incorrectly assigned as reporting on chemical exchange.

Rather than fit the resulting RD profiles from the 17 residues that 'passed' the chemical exchange criteria listed above to a global two-state exchange model, we first considered a subset of 5 that were the largest as defined as $R_{2,eff}(\nu_{CPMG} = 50\text{ Hz}) - R_{2,eff}(\nu_{CPMG} = 1000\text{ Hz})$ (>6 s^{-1}, 18.8 T). Extracted values of $k_{ex} = 160 \pm 40$ s^{-1} and $p_B = 4.9 \pm 0.9$ % were obtained that can be compared with $k_{ex} = 138 \pm 9$ s^{-1} and $p_B = 8.3 \pm 0.3$ % generated from fits of ^{15}N CPMG data. The discrepancies no doubt reflect the difficult in obtaining highly accurate exchange

parameters when only relatively small RD profiles are considered, as is the case for the ^{13}Cα dispersion curves (Fig. 3), but also the fact that in this relatively slow exchange regime k_{ex} and p_B are partly inversely correlated, which at least to some extent explains the higher k_{ex}/lower p_B values for ^{13}Cα relative to ^{15}N. The extracted values of (k_{ex}, p_B) obtained in this manner were subsequently used in global fits of all of the RD profiles to generate $|\Delta\varpi_{CPMG}|$ values, discussed below. It is worth noting that fixing (k_{ex}, p_B) did not lead to higher reduced χ^2 values relative to the case where exchange parameters were allowed to float in fits involving RD curves from all 17 residues, while the extracted exchange parameters were far more robust.

Figure 4 shows a bar graph of $|\Delta\varpi_{Direct}|$ (red) and $|\Delta\varpi_{CPMG}|$ (black) for all residues for which RD curves could be measured. Shown in the upper left hand corner is the pairwise root-mean-square-deviation (RMSD) between the two data sets. Note that $|\Delta\varpi_{CPMG}|$ was set to 0 for residues that were classified as 'lacking significant chemical exchange' by the criteria defined above. A good correlation is obtained between the two data sets, RMSD = 0.064 ppm (n = 44). The inset to the figure shows a linear correlation plot of $|\Delta\varpi_{CPMG}|$ *vs* $|\Delta\varpi_{Direct}|$, including only those residues with chemical exchange, for which an RMSD of 0.059 ppm was obtained.

A k_{ex} value of $\approx$150 s^{-1}, as obtained from analysis of the RD data sets described above, is on the 'slow side' for CPMG applications and we were interested in testing faster exchange regimes. To this end an additional aliquot of Ark1p peptide was titrated into the sample to increase the exchange rate. Values of $k_{ex} = 1030 \pm 50$ s^{-1} and $p_B = 89.4 \pm 0.8$ % were estimated from analysis of ^{15}N CPMG RD profiles recorded on the resulting sample, where p_B refers to the population of the peptide bound SH3 domain, as before. Subsequently, ^{13}Cα RD experiments were recorded at spectrometer field strengths of 14.1 T and 21.1 T and 18 residues identified for further analysis. Not surprisingly, the residues sensitive to the chemical exchange process were largely the same as before. In general, we find that it is possible to reliably identify conformational dynamics at ^{13}Cα positions if $|\Delta\varpi| > 0.2$ ppm and $100 < k_{ex} < 1000$ s^{-1}, with residues sometimes missed when $|\Delta\varpi|$ is smaller. CPMG RD profiles for exchanging residues were fitted to a global two-state process, using a similar procedure to that described above, with two such fits shown in Fig. 5.

Values of $k_{ex} = 930 \pm 50$ s^{-1}, $p_B = 87 \pm 2$ % agree well with $k_{ex} = 1030 \pm 50$ s^{-1}, $p_B = 89.4 \pm 0.8$ % from analysis of ^{15}N RD profiles and there is a good correlation between $|\Delta\varpi_{Direct}|$ and $|\Delta\varpi_{CPMG}|$ with an RMSD of 0.065 ppm for all residues for which RD profiles could be obtained (n = 44) and 0.060 ppm when including only the subset that are sensitive to the exchange process (Fig. 6).

Although the correlation between $|\Delta\varpi_{Direct}|$ and $|\Delta\varpi_{CPMG}|$ is excellent with $R_{Pearson} = 0.99$ (Fig. 6) it is also apparent that $|\Delta\varpi_{CPMG}|$ is consistently underestimated. This may reflect the small chemical shift differences that place the exchange regime in the fast limit for many of the residues, so that only the product $(1 - p_B)p_B(\Delta\omega)^2$ can be reliably estimated (Luz and Meiboom 1963). Palmer and coworkers have developed a method for establishing the exchange regime (Millet et al. 2000) by calculating α,

$$\alpha = \frac{B_{0,2} + B_{0,1}}{B_{0,2} - B_{0,1}} \cdot \frac{R_{ex,2} - R_{ex,1}}{R_{ex,2} + R_{ex,1}}$$

where $R_{ex,1}$, and $R_{ex,2}$ are the exchange contributions to transverse relaxation at static magnetic fields of $B_{0,1}$ and $B_{0,2}$, respectively. Values of α range between 0 and 2,

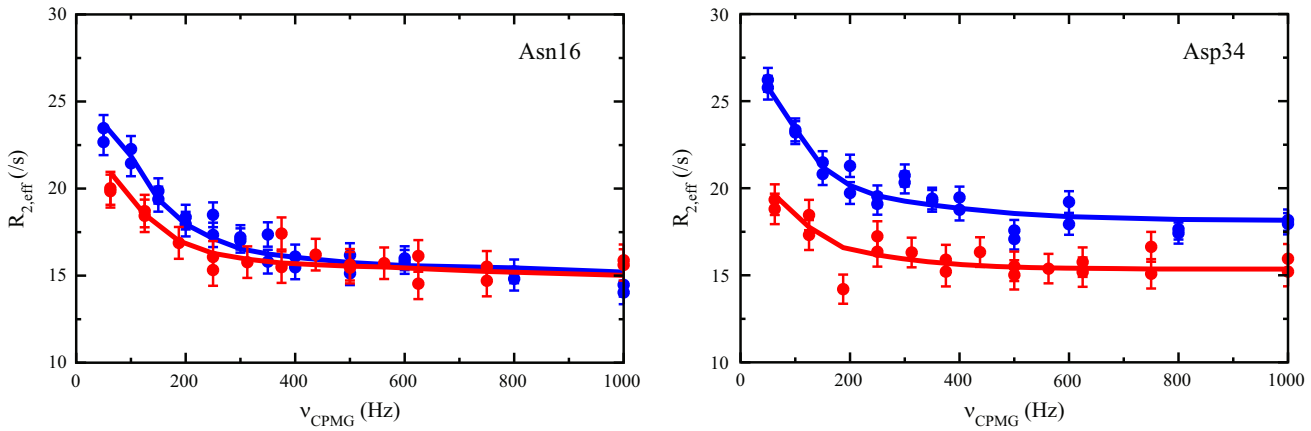

Fig. 3 Representative ^{13}Cα dispersion profiles for residues with significant chemical exchange in an Abp1p SH3 domain that interconverts between free and Ark1p peptide bound forms (≈5 % bound Ark1p peptide is present). The SH3 domain was produced with [2-^{13}C]-glycerol as the sole carbon source. *Red* (*blue*) symbols denote data points recorded at 14.1 (18.8) T, 25 °C, and the *solid lines* are a global fit to the data, assuming a model of two-site chemical exchange. See SI Figure S1 for data on all residues

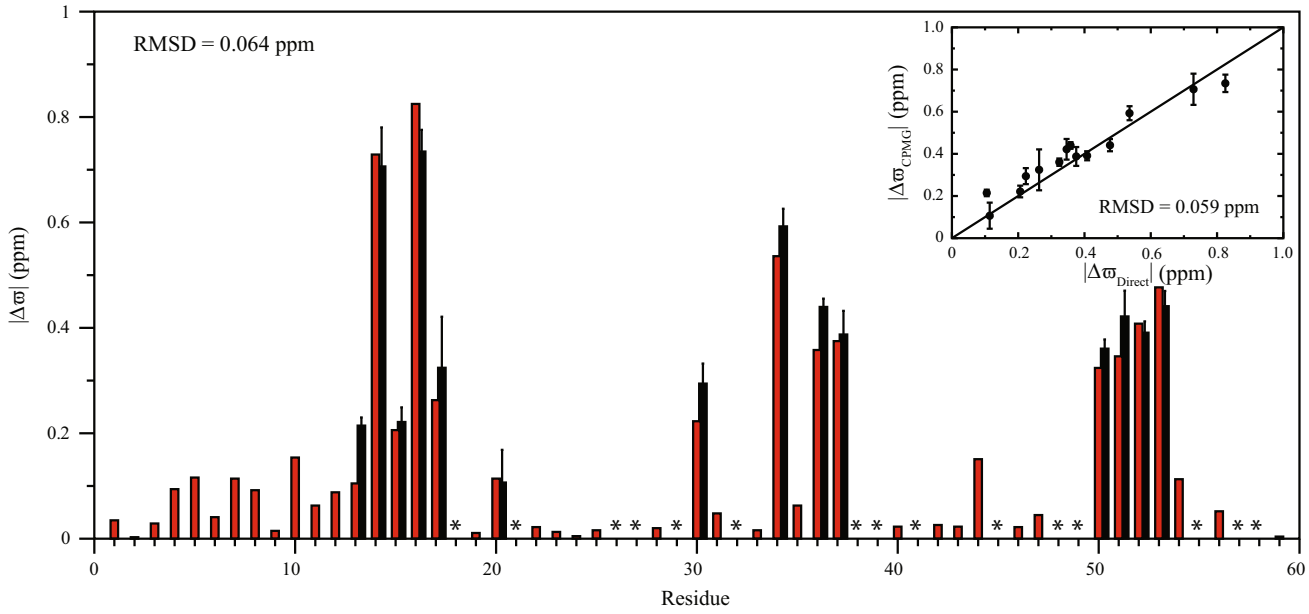

Fig. 4 Correlation between the absolute values of chemical shift differences between an Abp1p SH3 domain exchanging between free and Ark1 peptide bound forms, as measured in separate samples of free and fully bound protein (*red bars*), $|\Delta\varpi_{Direct}|$, and shift differences obtained from RD experiments measured on an SH3 domain sample with ≈5 % Ark1p peptide, $|\Delta\varpi_{CPMG}|$ (*black bars*). The pairwise RMSD between the data sets is indicated in the figure. The positions of Gly, Ile, Leu and Val residues that have been omitted from the analysis are indicated with *asterisks*. The *inset* shows the corresponding data for residues with 'significant' chemical exchange (see text) and the y = x line is included to guide the eye

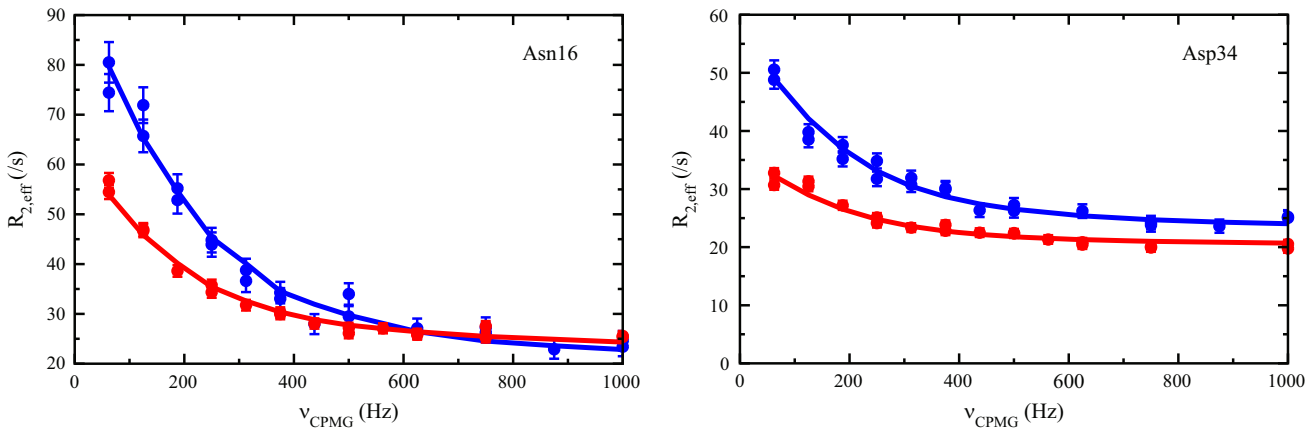

Fig. 5 RD profiles for the same residues as in Fig. 3 measured for a sample where ≈90 % Ark1p peptide has been included. *Red* (*blue*) symbols are data recorded at 14.1 (21.1) T, 25 °C, and the *solid lines* are best fits to a global two-site exchange process. See SI Figure S2 for data on all residues

where $\alpha < 1$, ≈ 1 and > 1 indicate slow, intermediate and fast exchange, respectively. In the present case, values between 1.40 and 1.97 are obtained with only one value below 1.50 (Asn16, $|\Delta\varpi| = 0.85$ ppm) and only three values below 1.80, indicating that the exchange regime approaches the fast limit. If k_{ex} and p_B are fixed to the values extracted from fits of ^{15}N RD profiles that include only those exchanging amide nitrogens with the largest $|\Delta\varpi|$ values (13 residues were used) and ^{13}Cα RD profiles fit again, the RMSD between $|\Delta\varpi_{Direct}|$ and $|\Delta\varpi_{CPMG}|$ decreases to 0.059 ppm (all residues; n = 44) and 0.035 ppm (exchanging residues). The slope of the best-fit line that passes the origin becomes 1.02 ± 0.02 compared to 0.86 ± 0.02 for the unrestrained fit.

For both of the exchange conditions considered here the values of $|\Delta\varpi_{CPMG}|$ correlate slightly worse with $|\Delta\varpi_{Direct}|$ than what we have obtained previously when experiments were measured on samples prepared with [2-^{13}C]-glucose as the carbon source. Then, an RMSD between $|\Delta\varpi_{CPMG}|$ and $|\Delta\varpi_{Direct}|$ of 0.04 ppm (exchanging residues only) was

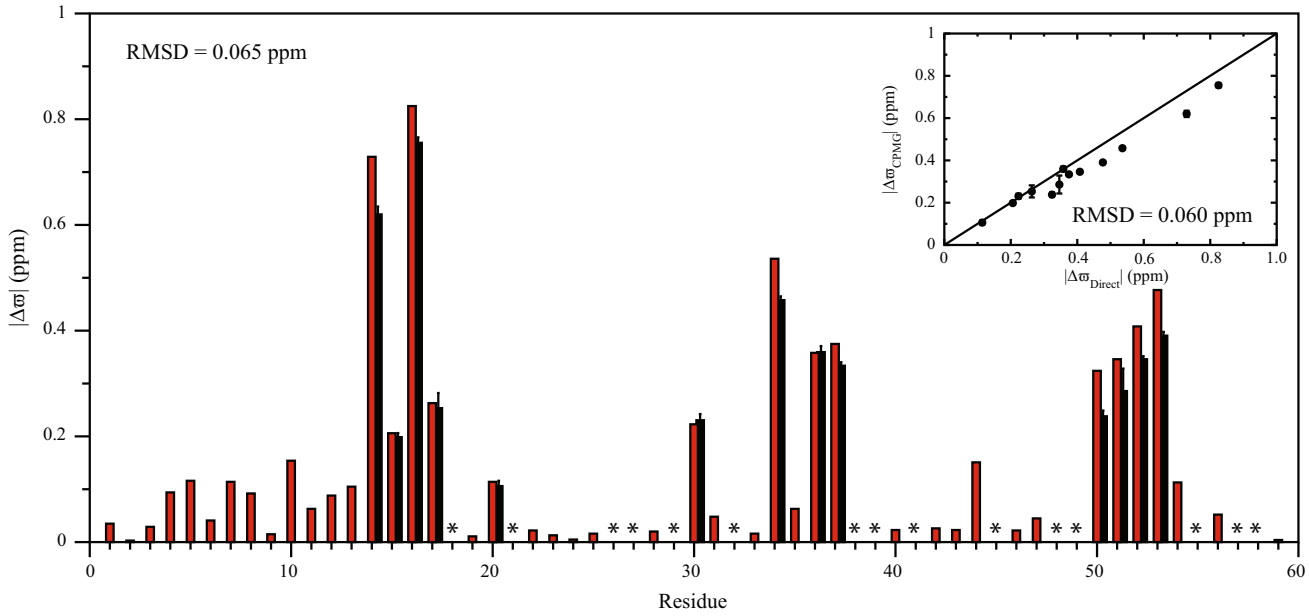

Fig. 6 Correlation between $|\Delta\varpi_{Direct}|$ and $|\Delta\varpi_{CPMG}|$, as in Fig. 4, for an SH3 domain sample with ≈90 % Ark1p peptide

obtained (Hansen et al. 2008). Although a protein concentration of 0.55 mM was used in the present study in comparison to 1.4 mM previously, the factor of two increase in concentration of ^{13}Cα spins from the present labeling scheme leads to experimental data sets with similar signal-to-noise ratios in both cases. The slight increase in error (corresponding to approximately 0.02 ppm) may well derive from the increase in the fraction of ^{13}Cα–^{13}Cβ spin pairs, leading to artifacts and slightly erroneous values especially when dispersions are small (as in the present application). Nevertheless, in comparison with average $\Delta\varpi$ values for random-coil to α-helix or β-strand transitions, 3.1 ± 0.9 ppm and −0.9 ± 0.4 ppm respectively (Wang and Jardetzky 2002), it is clear that the errors are well within the tolerance level for the reliable analysis of changes in secondary structure. Moreover, they are also within the accuracy of current chemical shift prediction programs (Shen and Bax 2010). Thus, ^{13}Cα shifts obtained in this manner can be used as restraints in structure calculations.

In summary, we have shown that protein expression using [2-^{13}C]-glycerol as the carbon source doubles the concentration of ^{13}C label at Cα relative to growths with [2-^{13}C]-glucose. However, unlike the case for [2-^{13}C]-glucose, there is a detectable fraction of unwanted ^{13}Cα–^{13}Cβ spin-pairs, especially for serine and residues for which serine is a precursor. Errors in ^{13}Cα chemical shifts obtained from fits of RD profiles are small compared to tolerance levels of current shift prediction programs. The present labeling strategy will be particularly useful for applications involving proteins that express poorly or that aggregate, where of necessity concentrations must be kept low and sensitivity, therefore, is limiting.

Acknowledgments We thank Dr. Martin Singull, Linköping University, for stimulating discussions and SWEDSTRUCT and the Swedish NMR Center for generous access to their high-field spectrometers. This work was supported by a grant from the Swedish Research Council (Dnr. 2012-5136) to P.L. L.E.K holds a Canadian Research Chair in Biochemistry.

References

Ahlner A, Carlsson M, Jonsson BH, Lundström P (2013) PINT—a software for integration of peak volumes and extraction of relaxation rates. J Biomol NMR 56:191–202

Auer R, Neudecker P, Muhandiram DR, Lundström P, Hansen DF, Konrat R, Kay LE (2009) Measuring the signs of ^{1}Ha chemical shift differences between ground and excited protein states by off-resonance spin-lock R_{1r} NMR spectroscopy. J Am Chem Soc 131:10832–10833

Bouvignies G, Vallurupalli P, Hansen DF, Correia BE, Lange O, Bah A, Vernon RM, Dahlquist FW, Baker D, Kay LE (2011) Solution structure of a minor and transiently formed state of a T4 lysozyme mutant. Nature 477:U111–U134

Bouvignies G, Vallurupalli P, Kay LE (2014) Visualizing side chains of invisible protein conformers by solution NMR. J Mol Biol 426:763–774

Carr HY, Purcell EM (1954) Effects of diffusion on free precession in nuclear magnetic resonance experiments. Phys Rev 94:630–638

Castellani F, van Rossum B, Diehl A, Schubert M, Rehbein K, Oschkinat H (2002) Structure of a protein determined by solid–state magic-angle-spinning NMR spectroscopy. Nature 420:98–102

Cavalli A, Salvatella X, Dobson CM, Vendruscolo M (2007) Protein structure determination from NMR chemical shifts. Proc Natl Acad Sci USA 104:9615–9620

Choy WY, Zhou Z, Bai YW, Kay LE (2005) An ^{15}N NMR spin relaxation dispersion study of the folding of a pair of engineered mutants of apocytochrome b_{562}. J Am Chem Soc 127:5066–5072

Delaglio F, Grzesiek S, Vuister GW, Zhu G, Pfeifer J, Bax A (1995) NMRPipe—a multidimensional spectral processing system based on unix pipes. J Biomol NMR 6:277–293

Dethoff EA, Petzold K, Chugh J, Casiano-Negroni A, Al-Hashimi HM (2012) Visualizing transient low-populated structures of RNA. Nature 491:724–728

Drubin DG, Mulholland J, Zhu ZM, Botstein D (1990) Homology of a yeast actin-binding protein to signal transduction proteins and myosin-I. Nature 343:288–290

Forsén S, Hoffman RA (1963) Study of moderately rapid chemical exchange reactions by means of nuclear magnetic double resonance. J Chem Phys 39:2892–2901

Geen H, Freeman R (1991) Band-selective radiofrequency pulses. J Magn Reson 93:93–141

Hansen DF, Vallurupalli P, Lundström P, Neudecker P, Kay LE (2008) Probing chemical shifts of invisible states of proteins with relaxation dispersion NMR spectroscopy: how well can we do? J Am Chem Soc 130:2667–2675

Haynes J, Garcia B, Stollar EJ, Rath A, Andrews BJ, Davidson AR (2007) The biologically relevant targets and binding affinity requirements for the function of the yeast actin-binding protein 1 Src-homology 3 domain vary with genetic context. Genetics 176:193–208

Ishima R, Torchia DA (2003) Extending the range of amide proton relaxation dispersion experiments in proteins using a constant-time relaxation-compensated CPMG approach. J Biomol NMR 25:243–248

Ishima R, Baber J, Louis JM, Torchia DA (2004) Carbonyl carbon transverse relaxation dispersion measurements and ms–ms timescale motion in a protein hydrogen bond network. J Biomol NMR 29:187–198

Kimsey IJ, Petzold K, Sathyamoorthy B, Stein ZW, Al-Hashimi HM (2015) Visualizing transient Watson-Crick-like mispairs in DNA and RNA duplexes. Nature 519:315–320

Korzhnev DM, Salvatella X, Vendruscolo M, Di Nardo AA, Davidson AR, Dobson CM, Kay LE (2004) Low-populated folding intermediates of Fyn SH3 characterized by relaxation dispersion NMR. Nature 430:586–590

Korzhnev DM, Religa TL, Banachewicz W, Fersht AR, Kay LE (2010) A transient and low-populated protein-folding intermediate at atomic resolution. Science 329:1312–1316

LeMaster DM, Kushlan DM (1996) Dynamical mapping of E. coli thioredoxin via ^{13}C NMR relaxation analysis. J Am Chem Soc 118:9255–9264

Lila T, Drubin DG (1997) Evidence for physical and functional interactions among two Saccharomyces cerevisiae SH3 domain proteins, an adenylyl cyclase-associated protein and the actin cytoskeleton. Mol Biol Cell 8:367–385

Loria JP, Rance M, Palmer AG 3rd (1999) A relaxation-compensated Carr-Purcell-Meiboom-Gill sequence for characterizing chemical exchange by NMR spectroscopy. J Am Chem Soc 121:2331–2332

Lundström P, Teilum K, Carstensen T, Bezsonova I, Wiesner S, Hansen DF, Religa TL, Akke M, Kay LE (2007) Fractional ^{13}C enrichment of isolated carbons using [1-^{13}C]- or [2-^{13}C]-glucose facilitates the accurate measurement of dynamics at backbone C^a and side-chain methyl positions in proteins. J Biomol NMR 38:199–212

Lundström P, Hansen DF, Kay LE (2008) Measurement of carbonyl chemical shifts of excited protein states by relaxation dispersion NMR spectroscopy: comparison between uniformly and selectively (13)C labeled samples. J Biomol NMR 42:35–47

Lundström P, Hansen DF, Vallurupalli P, Kay LE (2009a) Accurate measurement of alpha proton chemical shifts of excited protein states by relaxation dispersion NMR spectroscopy. J Am Chem Soc 131:1915–1926

Lundström P, Lin H, Kay LE (2009b) Measuring $^{13}C^b$ chemical shifts of invisible excited states in proteins by relaxation dispersion NMR spectroscopy. J Biomol NMR 44:139–155

Lundström P, Vallurupalli P, Hansen DF, Kay LE (2009c) Isotope labeling methods for studies of excited protein states by relaxation dispersion NMR spectroscopy. Nat Protoc 4:1641–1648

Luz Z, Meiboom S (1963) Nuclear magnetic resonance study of the protolysis of trimethylammonium ion in aqueous solution-order of the reaction with respect to solvent. J Chem Phys 39:366–370

Meiboom S, Gill D (1958) Modified spin-echo method for measuring nuclear relaxation times. Rev Sci Instrum 29:688–691

Millet O, Loria JP, Kroenke CD, Pons M, Palmer AG 3rd (2000) The static magnetic field dependence of chemical exchange line-broadening defines the NMR chemical shift time scale. J Am Chem Soc 122:2867–2877

Mulder FAA, Skrynnikov NR, Hon B, Dahlquist FW, Kay LE (2001) Measurement of slow (ms-ms) time scale dynamics in protein side chains by ^{15}N relaxation dispersion NMR spectroscopy: application to Asn and Gln residues in a cavity mutant of T4 lysozyme. J Am Chem Soc 123:967–975

Neudecker P, Robustelli P, Cavalli A, Walsh P, Lundström P, Zarrine-Afsar A, Sharpe S, Vendruscolo M, Kay LE (2012) Structure of an intermediate state in protein folding and aggregation. Science 336:362–366

Palmer AG 3rd, Kroenke CD, Loria JP (2001) Nuclear magnetic resonance methods for quantifying microsecond-to-millisecond motions in biological macromolecules. Methods Enzymol 339:204–238

Rath A, Davidson AR (2000) The design of a hyperstable mutant of the Abp1p SH3 domain by sequence alignment analysis. Protein Sci 9:2457–2469

Santoro J, King GC (1992) A constant-time 2D Overbodenhausen experiment for inverse correlation of isotopically enriched species. J Magn Reson 97:202–207

Shen Y, Bax A (2010) SPARTA plus: a modest improvement in empirical NMR chemical shift prediction by means of an artificial neural network. J Biomol NMR 48:13–22

Shen Y, Lange O, Delaglio F, Rossi P, Aramini JM, Liu GH, Eletsky A, Wu YB, Singarapu KK, Lemak A, Ignatchenko A, Arrowsmith CH, Szyperski T, Montelione GT, Baker D, Bax A (2008) Consistent blind protein structure generation from NMR chemical shift data. Proc Natl Acad Sci USA 105:4685–4690

Skrynnikov NR, Dahlquist FW, Kay LE (2002) Reconstructing NMR spectra of "invisible" excited protein states using HSQC and HMQC experiments. J Am Chem Soc 124:12352–12360

Vallurupalli P, Hansen DF, Stollar E, Meirovitch E, Kay LE (2007) Measurement of bond vector orientations in invisible excited states of proteins. Proc Natl Acad Sci USA 104:18473–18477

Vallurupalli P, Hansen DF, Kay LE (2008) Structures of invisible, excited protein states by relaxation dispersion NMR spectroscopy. Proc Natl Acad Sci USA 105:11766–11771

Vallurupalli P, Bouvignies G, Kay LE (2013) A computational study of the effects of ^{13}C-^{13}C scalar couplings on ^{13}C CEST NMR spectra: towards studies on a uniformly ^{13}C labeled protein. ChemBioChem 14:1709–1713

Voet D, Voet JG (1995) Biochemistry. Wiley, Hoboken

Vuister GW, Bax A (1992) Resolution enhancement and spectral editing of uniformly ^{13}C enriched proteins by homonuclear broad band ^{13}C decoupling. J Magn Reson 98:428–435

Wang YJ, Jardetzky O (2002) Probability-based protein secondary structure identification using combined NMR chemical-shift data. Protein Sci 11:852–861